A Smart Flexible Vital Signs and Sleep Monitoring Belt Based on MEMS Triaxial Accelerometer and Pressure Sensor

Chunhua He, Jiewen Tan, Xuelei Jian, Guangxiong Zhong, Lianglun Cheng, and Juze Lin

***Abstract*—People spend about one third of their lifetime in sleep, and sleep quality has a great impact on people's health. Therefore, vital signs and sleep quality monitoring are more and more important. In this article, a novel smart flexible sleep monitoring belt with MEMS triaxial accelerometer and pressure sensor is developed to detect vital signs, snore events, and sleep stages. Besides, the related algorithms and methods for data preprocessing, heart and respiration rates detection, snoring recognition, and sleep stages classification are proposed in detail. Then, a series of sleep experiments is performed based on the experimental platform for the smart flexible belt, and the test results measured by PolySomnoGraphy are used as the golden standards for comparison. The experimental results demonstrate that the detection accuracies of heart rate and respiration rate of the belt are about 1.5 and 0.7 bpm, respectively. The accuracy of 97.2% is achieved by the proposed snoring recognition method. In addition, as for 2-stage analysis, the sensitivities of awake and asleep stages are 90.2% and 100%, respectively; meanwhile, the corresponding accuracy of sleep stages prediction is as high as 95.1%. However, as for 4-stage analysis, the sensitivities of awake, rapid eye movement, light sleep, and deep sleep stages are 90.2%, 77.1%, 78.1%, and 73.5%, respectively; meanwhile, the corresponding accuracy of sleep stages prediction decreases to 79.7%. In general, the test results indicate that vital signs detection, snoring recognition, and sleep stages classification based on the sleep monitoring belt are feasible and effective. Hence, this smart flexible belt can be widely used for sleep monitoring at home due to low cost and high performance.**

***Index Terms*—Flexible belt, MEMS accelerometer, pressure sensor, snoring recognition, vital signs and sleep monitoring.**

Manuscript received 24 July 2021; revised 2 December 2021; accepted 24 January 2022. Date of publication 28 January 2022; date of current version 25 July 2022. This work was supported in part by the National Natural Science Foundation of China under Grant 62104047 and Grant U2001201. *(Corresponding author: Juze Lin.)*

Chunhua He is with the School of Computer, Guangdong University of Technology, Guangzhou 510000, China (e-mail: hechunhua@pku.edu.cn).

Jiewen Tan, Xuelei Jian, and Guangxiong Zhong are with the Research and Development Department, Guangzhou 37 Degree Smart Home Company Ltd., Guangzhou 510000, China (e-mail: tjw@37smarthome.com; jianxuelei@37smarthome.com; zhongguangxiong@37smarthome.com).

Lianglun Cheng is with the School of Computer, Guangdong University of Technology, Guangzhou 510000, China (e-mail: llcheng@gdut.edu.cn).

Juze Lin is with the Guangdong Provincial People's Hospital, Guangdong Academy of Medical Sciences, Guangzhou 510000, China (e-mail: 631753613@qq.com).

Digital Object Identifier 10.1109/JIOT.2022.3146926

I. Introduction

RECENTLY, there are more and more people with sleep disorders, and the decline of sleep quality makes most people disturbed and anxious [1]. Obtrusive sleep apnea (OSA) is one of the most important sleep disorders, which has a great impact on the sleep quality [2]. Sleep quality is related to age [3], cardiovascular, neurological, and psychosomatic conditions, which reflects the homeostasis status of autonomic nervous system (ANS) organization and circadian rhythms [4]. ANS is composed of the sympathetic and the parasympathetic nervous systems. Sleep stages mainly include rapid eye movement (REM) and various non-REM stages (NREM). NREM stages comprise awake, light sleep, and deep sleep stages [5]. Given that it is of great significance to evaluate the sleep quality, more and more research institutes pay attention to it and have proposed some effective and feasible methods of Internet of Things (IoT), including contact and noncontact, wearable, and nonwearable sleep monitoring schemes.

At present, the golden standard technique for assessing sleep quality is polysomnography (PSG), which is a combination of electroencephalography (EEG), electrocardiography (ECG), electrooculography (EOG), and electromyography (EMG) [6], [7]. However, it is time consuming, uncomfortable, obtrusive, and expensive. Although long-term wearable in-ear sensor can be adopted for recording the electroencephalogram (ear-EEG), the accuracy is not high enough yet [8], [9]. Smartphone can be used for OSA and sleep quality monitoring, nevertheless, it is power consuming and the test results are easily disturbed by ambient noises [10]–[12]. Even if OSA events can be detected by ultrasound sensor, it is also uncomfortable for the users to wear it on the neck [13].

Sleep positions have something to do with sleep quality; thus, smartphone, wristband, and chest band, composed of MEMS inertial measurement unit (IMU) or accelerometer, are utilized to collect the sleep data [14]–[16]. Whereas, it is uncomfortable for the users to wear these devices all night long. IMU or accelerometer, and piezoelectric sensor can be fixed under the mattress for sleep monitoring [17], [18], but it only detects the body movement accurately, rather than heart and respiration rates. In order to advance the sensitivity, a bed-mounted seismometer is utilized to measure heart and respiration rates [19], [20], but this scheme is high cost and the

sensitivity is apt to be affected by the structure and material of the bed.

Commercially, wrist sleep monitors, such as ActiWatch, can continuously monitor the sleep quality for multiple days [21]–[23], but it is difficult to accurately estimate different sleep stages merely based on the hands' movements. Even though the detection precision of a multimodal sensor system measuring hand's acceleration, ECG, and distal skin temperature outperforms that of ActiWatch, it still needs to be improved. On the other hand, a MEMS triaxial accelerometer and a pressure sensor can be combined together to fulfill sleep monitoring [24]. The former is applied to estimate the sleep pose and activity, while the latter is utilized to measure heart and respiratory rates. Sleep stages are identified based on heart rate and activity, while sleep quality is evaluated by sleep pose, sleep apnea, and sleep time. But it is a redundancy design because accelerometer can be adopted to measure heart and respiratory rates.

Flexible and thin sensor materials are very useful for physiological applications where the sensor is in contact with the body directly or indirectly [25]. The sensor is integrated into clothing, chair, bed sheet, mattress, or bed, which is designed to be as unobtrusive and comfortable for the users as possible. Nowadays, some polyvinylidenefluoride (PVDF) film and electromechanical film (EMF) materials are widely used in physiological measurement systems to detect the heart and respiration rates, as well as sleep movement [26], [27]. The sensitivities of both materials are high enough to sense the super weak physiological signals of vibration and vital signs [28], [29]. Nevertheless, there are some inevitable misjudgments about in-and-out-of-bed activities for a sole sensor without other sensors' fusion. Although EMFs and load cells can be merged into the bed to acquire vital signs, body movements, and in-and-out-of-bed activities [30], the cost of the bed or mattress is very high. Similarly, a piezoelectric ceramic sensor is mounted in the cavity of the pillow made of shape memory foam for sleep monitoring [31], [32]; although the detection sensitivity is high, the pillow's cost is also high. In order to further enhance the sensitivity, laser blood flowmeter and optical fiber interferometer are embedded in the mattress or bed for sleep monitoring [33]–[35]. However, the cost is more expensive than those of the formers.

In addition, there are three common noncontact and long-distance sleep detection approaches, namely, camera, radar, and WiFi schemes. Sleep process can be recorded by infrared cameras, and then, the respiratory rate and posture are estimated based on the videos [36], [37]. Nevertheless, the high cost induced by multiple infrared cameras makes it difficult to promote the application. Furthermore, the users will inevitably worry about privacy issues resulted from the cameras. Radio-frequency (RF) sensors, such as single-tone continuous-wave (CW, also called Doppler radar), frequency-modulated CW (FMCW), impulse radio ultrawide band (IR-UWB), and millimeter wave radar sensors, are similarly applied to monitor the sleep quality and vital signs [38]–[41]. Generally, the detection accuracies are very high, but apt to be interfered by multiple persons in the same space. Although the WiFi transmitter and receiver can be used to detect the respiration rate and posture during sleep [42]–[45], it cannot monitor the heart rate.

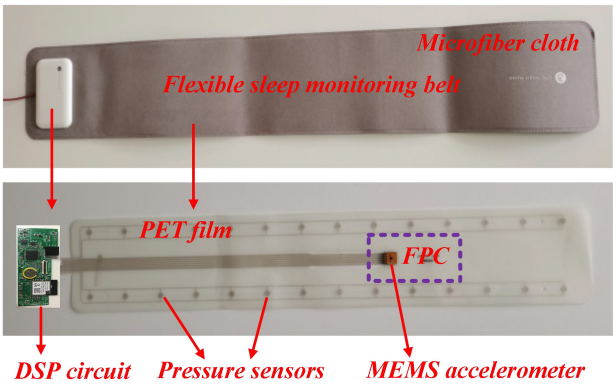

Fig. 1. Photograph of a smart flexible belt.

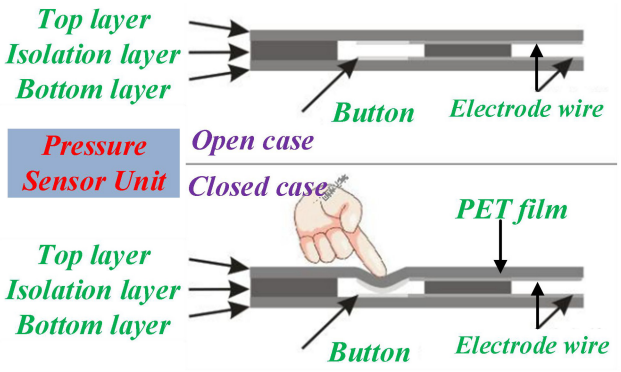

Fig. 2. Structure and operation principle of a pressure sensor unit.

Hence, in order to achieve high performance, low cost, and comfortable experience, this article will propose a smart flexible vital signs and sleep monitoring belt based on MEMS triaxial accelerometer and pressure sensor, followed by detection and analysis methods. It can be applied to detect heart and respiratory rates, body movement, in-and-out-of-bed activity, and snore event, which will be applied to further estimate the sleep stages and sleep quality.

II. System Design for Flexible Belt

The picture of a smart flexible belt is shown in Fig. 1. It is mainly composed of a digital signal processor (DSP) circuit and a flexible sensor film. The belt is packaged by microfiber cloth, which is thin and has a better texture. Due to the large friction, it is not easy to be moved when the belt is placed on the mattress. The flexible polyethylene terephthalate (PET) film inside the belt consists of a pressure sensor array and a MEMS triaxial accelerometer. The accelerometer is mounted on a flexible printed circuit (FPC), which is fixed on the top of the film with double faced adhesive tape. The wires or electrodes in the film are fabricated with silver paste, which can guarantee that the maximum resistance of the wires is less than 20 Ω.

The structure and operation principle of a pressure sensor unit are shown in Fig. 2. The top layer and bottom layer are both PET materials, while the isolation layer is

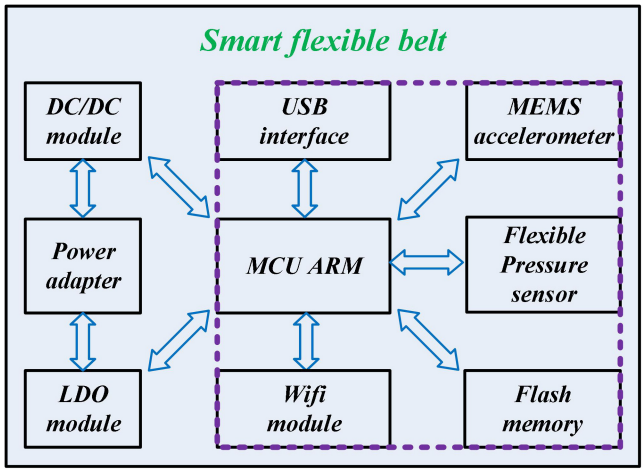

Fig. 3. System overview for a smart flexible belt.

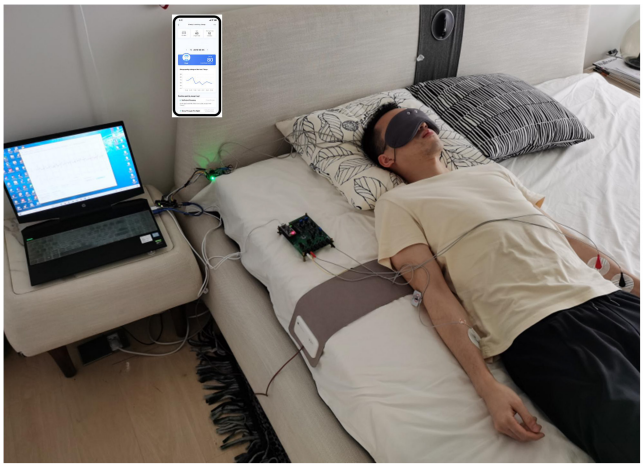

Fig. 4. Experimental platform for the smart flexible belt.

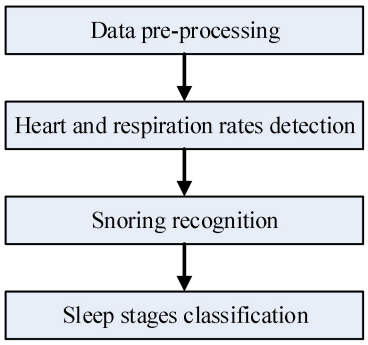

Fig. 5. Flowchart of vital signs detection and sleep stages classification.

the double faced adhesive tape. The size of a PET film is 13 cm × 75 cm × 0.025 cm, and the adhesive force is more than 15N/25 mm. The insulation resistance is bigger than 100 MΩ, and the tolerant voltage is 250 VRms. The threshold of the pressure sensor unit is designed to be 20 gf, which can filter the interferences induced by some quilts and mats. That is, once the force exerted to the button is larger than 20 gf, the pressure switch is on, otherwise, it is off, as shown in Fig. 2. Hence, based on the output of this pressure sensor array, it is easy to judge whether there is a person or a heavy object pressing on the flexible belt. Combined with the vital signs measured by the MEMS accelerometer, the in-and-out-of-bed state of the user can be recognized.

The overview of the DSP circuit system is depicted in Fig. 3, which mainly includes three subsystems, namely, power supply subsystem, processor subsystem, and sensor subsystem.

1) *Power Supply Subsystem:* Dc/dc converter, low dropout regulator (LDO), and power adapter are applied to generate the appropriate supply voltages to the other subsystems.
2) *Processor Subsystem:* STM32F411 ARM is chosen as the core microprogrammed control unit (MCU), which has enough resources to achieve the key algorithms of vital signs detection, snoring recognition, and sleep stages classification. USB interface is utilized to connect with personal computer (PC), while the WiFi module is used to achieve the IoT communication. Flash memory is applied to save the log data and sleep results for the last month.
3) *Sensor Subsystem:* A triaxial MEMS accelerometer ISM330DLC is adopted to acquire the weak vibration signals, which can be applied to extract the heart and respiratory rates, body movement, snore event, and so on. This sensor is the core of the belt. Besides, a pressure sensor array realized in the flexible belt is applied to detect the in-and-out-of-bed state of a user.

The experimental platform for the smart flexible belt is set up after the system design, as shown in Fig. 4. Based on this test platform, a series of sleep experiments can be performed.

III. Sleep Analysis Methods

The flowchart of vital signs detection and sleep stages classification is shown in Fig. 5. The proposed analysis methods mainly include the methods of data preprocessing, heart and respiration rates detection, snoring recognition, and sleep stages classification, and the detailed description is as follows.

A. Data Preprocessing Method

In this article, the x-axis acceleration signal is adopted for vital signs analysis, and the original acceleration signal (ACC) is depicted in the first subgraph of Fig. 6. It demonstrates that the noise is a little big, and the respiration signal is far larger than the heart rate signal. In order to advance the detection accuracy, envelope and details extractions are very important. Envelope signal containing respiratory information is a low-frequency signal, while details signal containing heart rate information is relatively a high-frequency signal. Given that low-pass filter (LPF) can be applied to distinguish the envelope signal from details signal, this article adopts a second-order LPF to conduct the extractions because it is simple and easy to implement. The transfer function of the LPF is described as

$$\frac{Y[s]}{X[s]} = \frac{\omega_0^2}{s^2 + 2\xi_0\omega_0 s + \omega_0^2} \tag{1}$$

where complex frequency s is equal to $j\omega$, and ω stands for the angular frequency. ω_0 and ξ_0 are the cut-off angular frequency

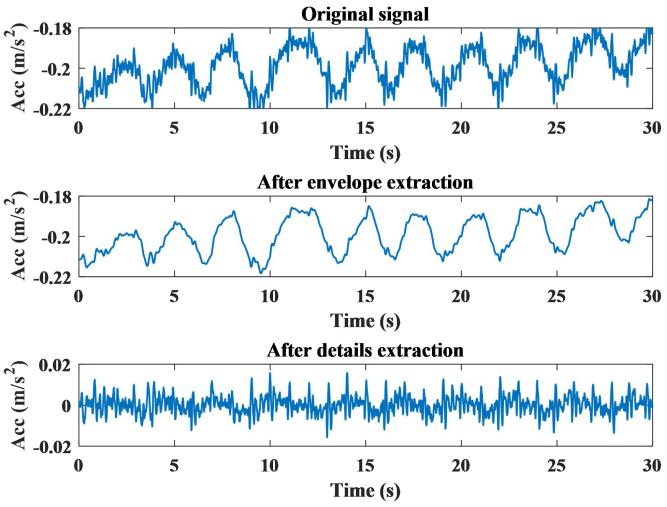

Fig. 6. Envelope and details signals are extracted from the original signal.

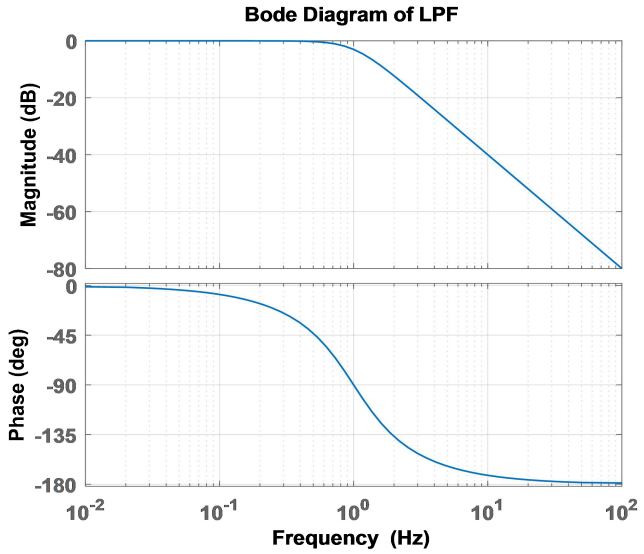

Fig. 7. Bode diagram of a second-order low pass filter.

and damping ratio of a second-order LPF. Y and X are the output signal and input signal, respectively. Here, the cut-off frequency is set to be 2 Hz, and ξ_0 is set to be 0.707. Thus, the bode diagram of the LPF is illustrated in Fig. 7. After bilinear transformation with (2), the transfer function in the discrete frequency domain (z domain) can be derived as (3)

$$s = \frac{2f_s(z-1)}{z+1} \tag{2}$$

$$\frac{Y[z]}{X[z]} = \frac{\omega_0^2(1+2z^{-1}+z^{-2})}{(4f_s^2+4\xi_0\omega_0 f_s+\omega_0^2)+2(\omega_0^2-4f_s^2)z^{-1}+(4f_s^2-4\xi_0\omega_0 f_s+\omega_0^2)z^{-2}} \tag{3}$$

where f_s represents the sampling rate, which is set to be 125 Hz in this article. Based on (3), the LPF is easy to implement in the MCU. Therefore, the envelope signal is extracted after LPF processing, and the details signal is accordingly obtained by subtracting the envelope signal from the original signal, as depicted in Fig. 6.

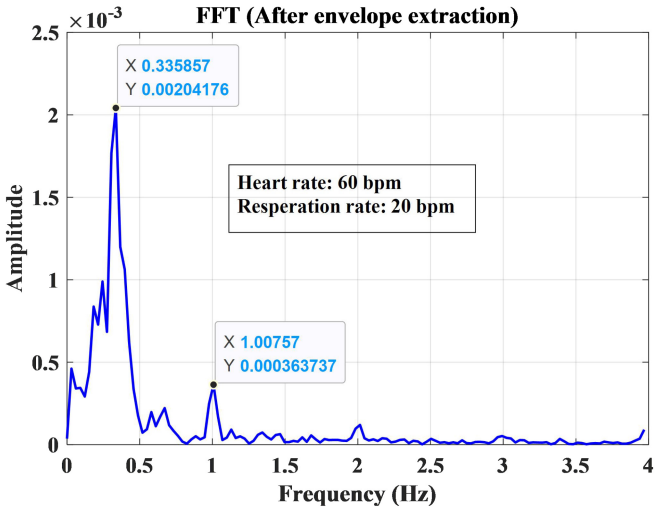

Fig. 8. FFT spectrum of the envelope signal.

B. Heart and Respiration Rates Detection Method

Once there is someone or something pressing on the belt, the corresponding acceleration signal is acquired, and the envelope signal and details signal are accordingly obtained. Then, the heart and respiration rates can be calculated after fast Fourier transform (FFT) processing. Before that, these signals should be processed by a Hanning window function, whose formula is

$$W[i] = \left[1-\cos\left(\frac{2\pi i}{L}\right)\right]/2,\ 1 \le i \le L \tag{4}$$

where L is the length of the window. Compared with the rectangular window function, the Hanning window can weaken the side-lobe size and spectrum leakage. After processing with the Hanning window function, FFT spectrum analysis is conducted, and the formula is as follows:

$$Y[k] = \sum_{i=1}^{N} y[i]e^{-j2\pi ki/N},\ 1 \le k \le N \tag{5}$$

where N is the length of the input vector. Here, it is set to be 4096. Thus, the valid amount of data of each frame after FFT processing is 2048. The FFT spectrums of the envelope signal and details signal are shown in Figs. 8 and 9, respectively. Considering that the heartbeat frequency is generally between 0.07 and 0.7 Hz, and the breathing frequency is generally between 0.7 and 2.0 Hz, hence, the frequency corresponding to the peak of amplitude response of the envelope signal between 0.07 and 0.7 Hz is taken as the breathing frequency (f_{pr}), as shown in Fig. 8. Likewise, the frequency corresponding to the peak of amplitude response of the details signal between 0.7 and 2 Hz is taken as the heartbeat frequency (f_{ph}), as shown in Fig. 9. Heart rate (HR) and respiration rate (RR) stand for the times of occurrence in a minute, and the units are beats per minute and breaths per minute, respectively, both abbreviated as bpm. Take Figs. 8 and 9 as example, the heart rate and respiration rate are calculated to be 60 and 20 bpm, respectively, which are pretty normal.

By comparison, it can be seen that the breathing peak in Fig. 8 is much larger than the heartbeat peak, while the two

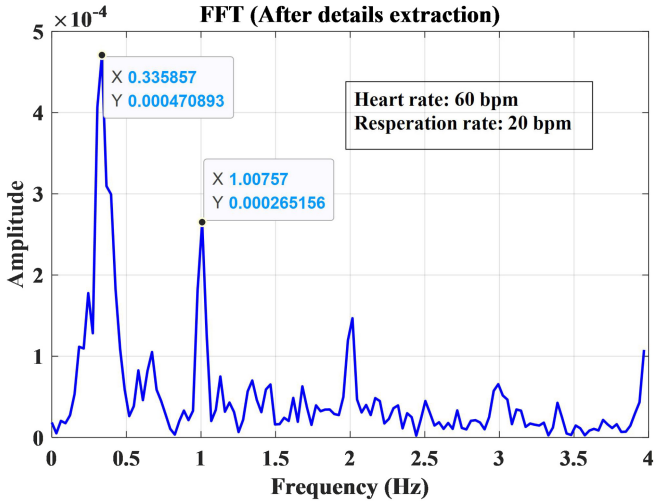

Fig. 9. FFT spectrum of the details signal.

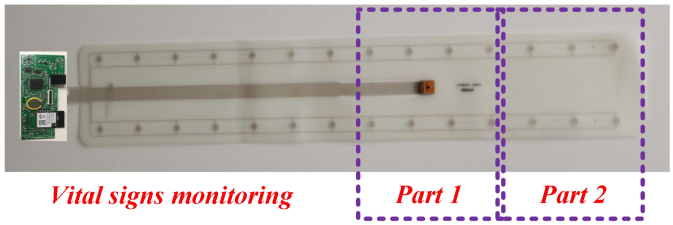

Fig. 10. Someone may lie on the position of Part 1 or Part 2, and the accelerometer may be fixed on the upper or lower surface of the belt.

TABLE I
TEST RESULTS OF RESPIRATION RATE AND PEAK IN DIFFERENT CASES

Location	Position	Respiration rate RR (bpm)	Breathing peak P_{RR}
Upper	Part 1	20	0.003199
Lower	Part 1	19	0.00234
Upper	Part 2	20	0.000453
Lower	Part 2	19	0.000319

peaks in Fig. 9 are close, indicating that envelope or details extraction can effectively enhance the signal intensity of the frequency band of interest, thereby improving the detection accuracies of heart rate and respiration rate. It must be noted that lying on different positions of the monitoring belt will lead to different signal intensities, and the signal intensities are also different when the accelerometer is fixed on the upper surface or the lower surface of the monitoring belt. For example, someone may lie on the position of Part 1 (the middle of the belt) or Part 2 (the edge of the belt), and the accelerometer may be fixed on the upper surface or the lower surface of the belt, as shown in Fig. 10. In different cases, HR and RR, as well as the heartbeat peak (P_{HR}) and breathing peak (P_{RR}), are measured for the same person, as depicted in Tables I and II, respectively.

The experimental results demonstrate that the heartbeat peaks and breathing peaks of the case when the accelerometer is fixed on the upper surface of the belt are a little larger than those of the case when the accelerometer is fixed on the lower surface of the belt. Therefore, the accelerometer is finally fixed

TABLE II
TEST RESULTS OF HEART RATE AND PEAK IN DIFFERENT CASES

Location	Position	Heart rate HR (bpm)	Heartbeat peak P_{HR}
Upper	Part 1	60	0.000472
Lower	Part 1	61	0.000346
Upper	Part 2	60	0.000061
Lower	Part 2	61	0.000047

on the upper surface of the belt in this article. In addition, the heartbeat peaks and breathing peaks of Part 1 are about an order of magnitude larger than those of Part 2. However, owing to adopting FFT analysis, the changes of signal intensity induced by the mentioned cases hardly affect the test results of heart rate and respiration rate since the differences are less than 1 bpm.

In order to avoid misjudgment, if P_{HR} and P_{RR} are less than the preset thresholds (P_{HR0}) and (P_{RR0}), respectively, it is judged that there are no meaningful vital signs (i.e., the heart rate and respiration rate). Given that the signal intensity of Part 2 is less than that of other part, thus the signal of Part 2 will be applied to confirm the thresholds. The setting rule of P_{HR0} and P_{RR0} is as follows. First, enter the calibration mode through the smartphone APP settings, and then the user lies awake on the Part 2 of the monitoring belt and breathes naturally for about 2 min. After the heartbeat and breathing ease, calculate the heartbeat peak and breathing peak in the frequency bands of 0.07–0.7 Hz and 0.7–2.0 Hz, respectively. Then, half of these two values are used as the preset thresholds (P_{HR0} and P_{RR0}) recorded to the flash memory. Finally, the APP exits calibration mode and returns to normal mode. Hence, the equations of HR and RR can be described as

$$\mathrm{HR} = \begin{cases} 60 \times f_{\mathrm{ph}}, P_{\mathrm{HR}} \geq P_{\mathrm{HR0}} \\ 0, P_{\mathrm{HR}} < P_{\mathrm{HR0}} \end{cases} \tag{6}$$

$$\mathrm{RR} = \begin{cases} 60 \times f_{\mathrm{pr}}, P_{\mathrm{RR}} \geq P_{\mathrm{RR0}} \\ 0, P_{\mathrm{RR}} < P_{\mathrm{RR0}}. \end{cases} \tag{7}$$

C. Snoring Recognition Method

In order to better evaluate the sleep quality, the detection of snore event is necessary. Thereby, snoring recognition based on the envelope signal is of great significance. Obviously, for the same person, the respiration rate of the snoring signal is less than that of nonsnoring signal since apnea will occur when snoring. Furthermore, the peak-to-peak value of the respiratory wave of the snoring signal is larger than that of nonsnoring signal because the breathing force increases intermittently once snoring. The time-domain original signals and FFT spectrums of snoring and nonsnoring are depicted in Figs. 11 and 12, respectively. The test results indicate that the respiration rate of snoring signal is indeed less than that of the nonsnoring signal, while the breathing peak of snoring signal is larger than that of nonsnoring signal, which accords with the analysis above.

Therefore, snoring recognition can be achieved based on this principle, that is, if the respiration rate (RR) is less than the preset threshold (RR_1) and the breathing peak (P_{RR}) in the FFT spectrum is larger than the preset threshold (P_{RR1}),

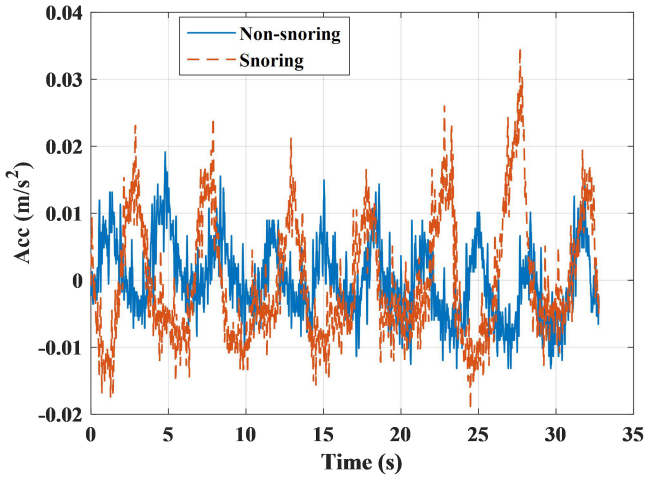

Fig. 11. Time-domain original signals of snoring and nonsnoring.

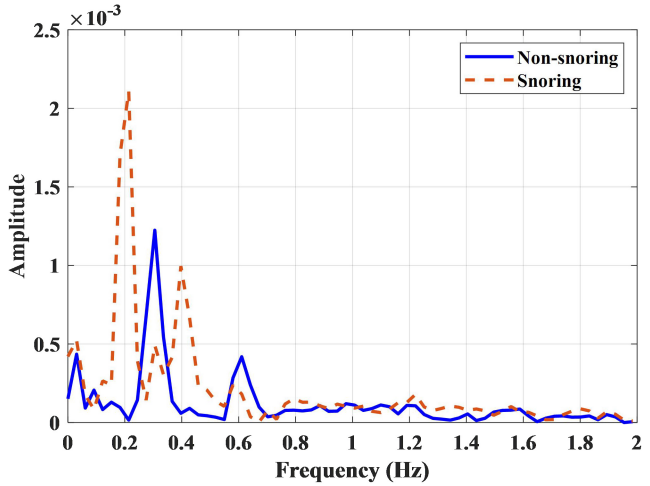

Fig. 12. FFT spectrums of the envelope signals of the snoring and nonsnoring signals.

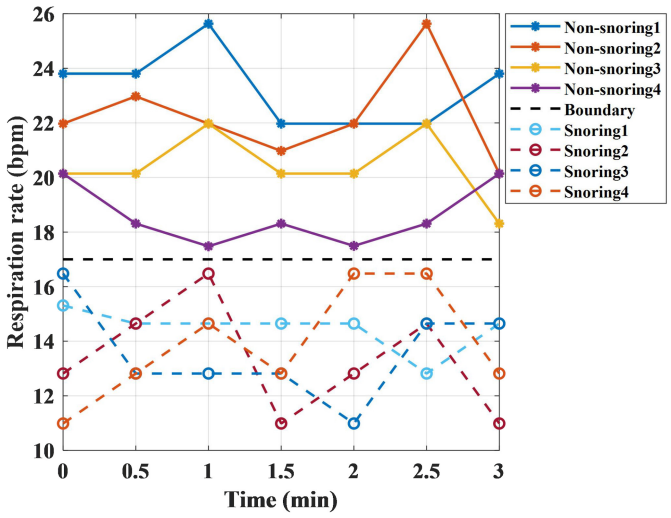

Fig. 13. Respiration rates of four persons in the snoring and nonsnoring stages.

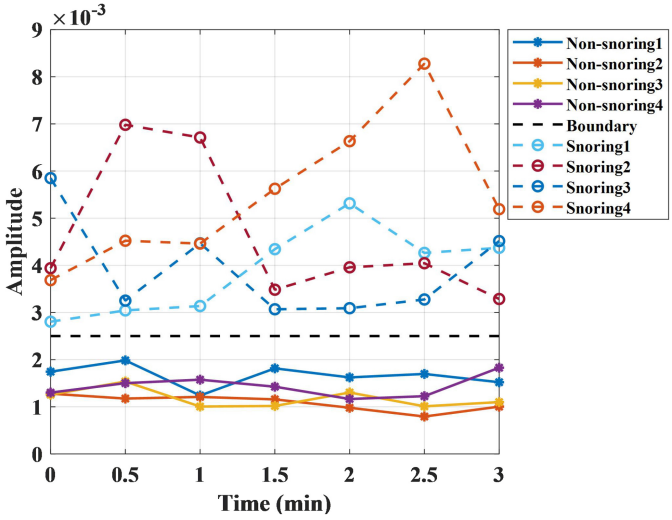

Fig. 14. Breathing peaks of four persons with and without snoring.

it is judged that there are snore events in the acquired signal, otherwise, there are no snore events. The respiration rates of four persons in the snoring and nonsnoring stages are measured by the monitoring belt within 3 min, as shown in Fig. 13. Meanwhile, the corresponding breathing peaks of four persons in the snoring and nonsnoring stages are shown in Fig. 14. The fluctuations and averages of breathing peak vectors of snoring signals are both larger than those of nonsnoring signals; it means the standard deviations and averages of breathing peak vectors in a short period (such as 3 min) can be regarded as the features for snoring recognition. In short, Figs. 13 and 14 indicate that the experimental results accord with the analysis above.

Even though the signal intensities of different positions of the belt are different, it does not affect the detection accuracy of RR; however, the change of P_{RR} induced by the change of sleep position maybe affect the results of snoring recognition. Considering that snoring and the change of sleep position both affect P_{RR}, so it is impossible to judge whether snoring exists only by the change of P_{RR}. Therefore, the effect of sleeping position on the belt should be eliminated for advancing the accuracy of snoring recognition. Fortunately, the fluctuations and averages of breathing peak vectors are both related to sleep position, and the enhancement or attenuation brought by sleep position is basically the same for both. Therefore, the influence of sleep position can be removed by dividing the standard deviation of breathing peak vector in a short period (such as 3 min) by the corresponding average, that is, the quotient (Q) is taken as the feature of the signal. To sum up, Q combined with RR within 3 min can be used for snoring recognition.

D. Sleep Stages Classification Method

Sleep stages are mainly includes four stages, namely, awake, light sleep, deep sleep, and REM, which are associated with the changes of heart rate and body movement. As mentioned above, the in-and-out-of-bed state of a user can be recognized based on the respiration rate and the output (PP) of the pressure sensor array. All the pressure sensor units are connected in parallel, that is, as long as the button of any pressure sensor unit is pressed, the switch is on, and PP is high level (i.e., 1),

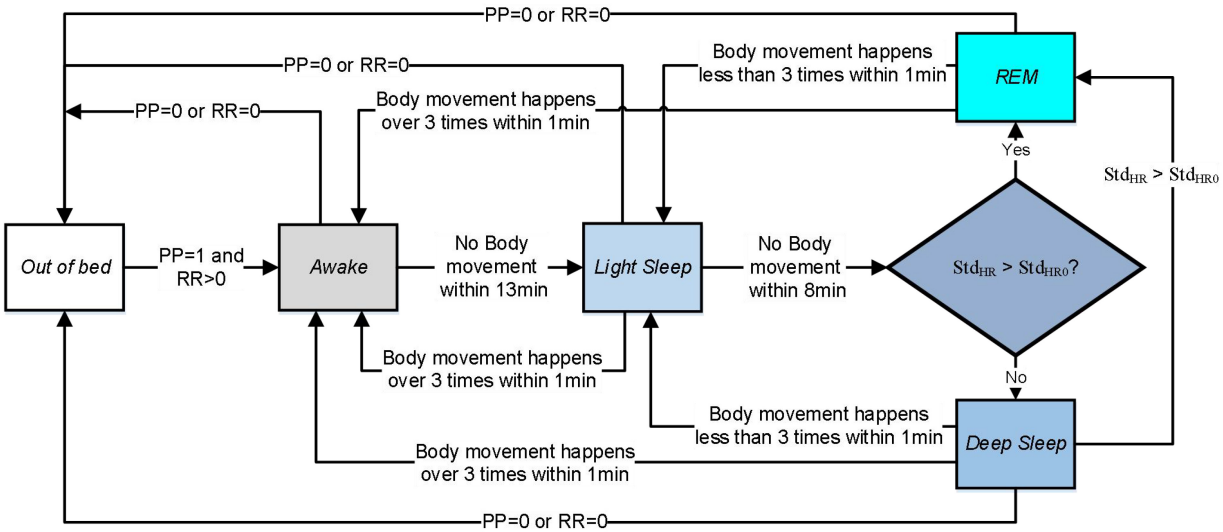

Fig. 15. Classification and predicted method of four sleep stages.

otherwise, PP is low level (i.e., 0). In order to eliminate the influence of foreign objects, respiration rate is combined to judge whether there is a person or a heavy object pressing on the flexible belt. Therefore, the expression of sleep status can be derived as

$$\text{status} = \begin{cases} \text{in bed}, & \text{PP} = 1 \text{ and } \text{RR} > 0 \\ \text{out of bed}, & \text{PP} = 0 \text{ or } \text{RR} = 0. \end{cases} \tag{8}$$

Once someone is detected lying on the monitoring belt, the judgment of sleep stages will start. If the acceleration (ACC) measured by the MEMS accelerometer is larger than the preset threshold (ACC_0), then it is judged that there are some body movements, *vice versa*. The standard deviation of heart rates in the last 20 s is recorded as Std_{HR}, and the corresponding preset threshold is Std_{HR0}. In this article, ACC_0 and Std_{HR0} are set 0.3 m/s^2 and 5.4 bpm, respectively. Hence, the classification and predicted method of four sleep stages can be illustrated in Fig. 15. The detailed description of the sleep stage (SS) is as follows.

1) *Awake Stage:* As soon as someone lies on the belt, SS is set to be awake stage immediately. If there is no body movement within 13 min, SS is set to be light sleep stage.
2) *Light Sleep Stage:* If there is no body movement within 8 min and $\text{Std}_{\text{HR}} > \text{Std}_{\text{HR0}}$, SS is set to be REM stage. If there is no body movement within 8 min and $\text{Std}_{\text{HR}} \leq \text{Std}_{\text{HR0}}$, SS is set to be the deep sleep stage. If body movement happens over three times within 1 min, SS is set to be awake stage.
3) *Deep Sleep Stage:* If $\text{Std}_{\text{HR}} > \text{Std}_{\text{HR0}}$, SS is set to be REM stage. Else, if body movement happens over three times within 1 min, SS is set to be awake stage, otherwise, SS is set to be light sleep stage.
4) *REM Stage:* If body movement happens over three times within 1 min, SS is set to be awake stage, otherwise, SS is set to be light sleep stage.
5) *Out of Bed:* Whatever SS is, if PP = 0 or RR = 0, SS will be set to be void, and sleep status is out of bed.

Hence, sleep stages can be predicted and classified according to these rules, and the analysis results will be compared with those detected by PSG.

IV. Experimental Results

A series of sleep experiments is performed based on the experimental platform for the smart flexible belt, as shown in Fig. 4. Since the smart belt is an IoT product, the test results can be also obtained by the APP in a smartphone. The detection accuracies of heart rate, respiration rate, snoring event, and sleep stages are so important that three types of experiments are performed in this section.

Before starting the experiments, the flexible belt is placed on the mattress, and a thin bedsheet or mat can be placed on the top of the belt and mattress. Then, the tested person lies on the top of the bed, and the flexible belt is underneath the chest. For comparison, PSG is applied for the synchronous tests.

A. Heart and Respiration Rates Detection

In order to evaluate the accuracies of vital signs measured by the sleep monitoring belt, the results measured by PSG are used as the golden standards. Therefore, the relevant parameters of the tested person are acquired by the sleep monitoring belt and PSG at the same time. The data of 1 h are acquired for the analysis, and the heart rate and respiration rate are computed every minute. Afterward, statistical analysis is adopted to evaluate the detection accuracies.

The curves of heart rate and respiration rate measured by the sleep monitoring belt and PSG within 1 h are shown in Figs. 16 and 17, respectively. It figures out that the standard deviation of the differences between the two heart rate curves is 1.5 bpm, while the maximum difference is 3 bpm. In addition, the standard deviation of the differences between the two respiration rate curves is 0.7 bpm, while the maximum difference is 1 bpm. Thus, the accuracies of vital signs measured by the sleep monitoring belt are good, which benefits the following snoring recognition and sleep stages classification.

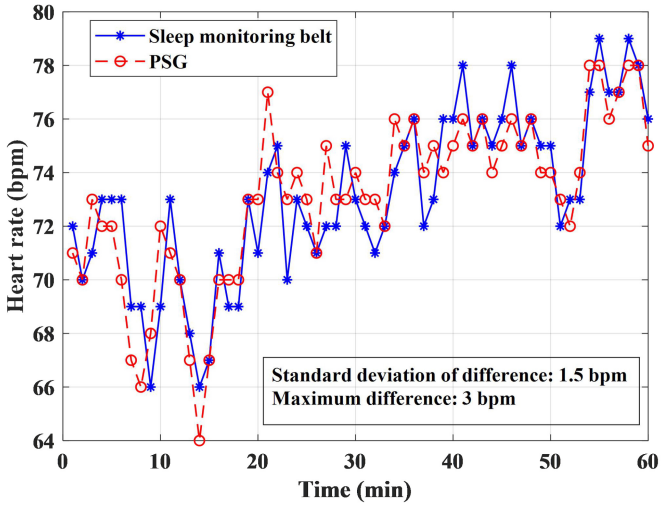

Fig. 16. Curves of heart rate are measured by the sleep monitoring belt and PSG within 1 h.

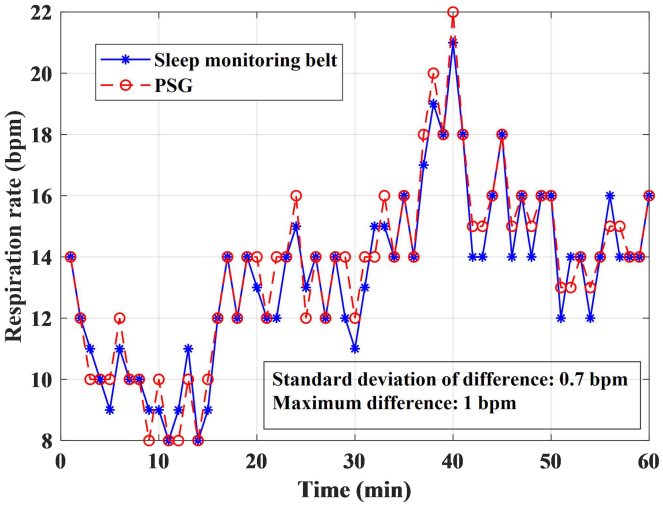

Fig. 17. Curves of respiration rate are measured by the sleep monitoring belt and PSG within 1 h.

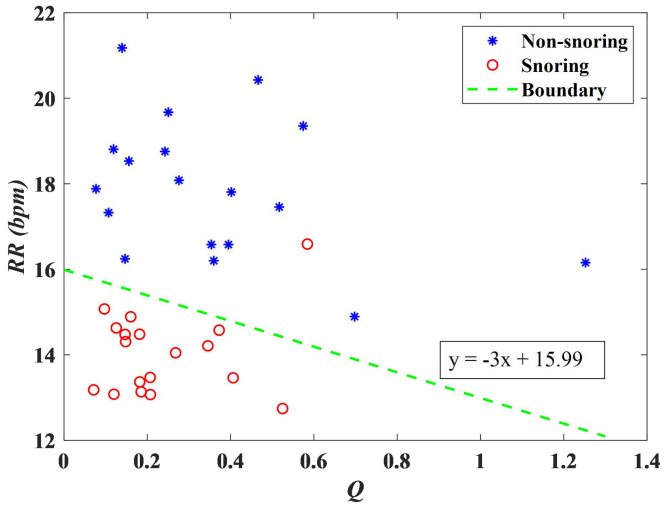

Fig. 18. Snoring recognition and clustering based on RR and Q.

B. Snoring Recognition

As mentioned above, a pair of Q and RR can be obtained every 3 min, so 18 pairs of data can be obtained in 54 min, which are depicted in Fig. 18. It indicates that the distributions of the snoring and nonsnoring data are obviously different. Taking the dashed green line (whose formula is $y = -3x + 15.99$) as the boundary, the data points above the green line are judged as the nonsnoring cluster, while the data points below the green line are judged as the snoring cluster. Therefore, the clustering rule is as follows:

$$\text{cluster} = \begin{cases} \text{non-snoring}, & 3Q + \text{RR} - 15.99 \geq 0 \\ \text{snoring}, & 3Q + \text{RR} - 15.99 < 0. \end{cases} \quad (9)$$

It can be seen that the nonsnoring events are correctly identified, but one of the snoring events is misjudged. Define that true positive (TP) is the number of correctly detected abnormal epochs (i.e., snore), true negative (TN) is the number of correctly detected normal epochs (i.e., nonsnore), false positive (FP) is the number of incorrectly detected abnormal epochs (i.e., snore), and false negative (FN) is the number of incorrectly detected normal epochs (i.e., nonsnore). Thus, the recognition sensitivity (Se), specificity (Sp), accuracy (Ac), and error (Er) can be defined as follows:

$$\begin{aligned} \text{Se} &= \text{TP}/(\text{TP} + \text{FN}) \\ \text{Sp} &= \text{TN}/(\text{TN} + \text{FP}) \\ \text{Ac} &= (\text{TP} + \text{TN})/(\text{TP} + \text{TN} + \text{FP} + \text{FN}) \\ \text{Er} &= (\text{FP} + \text{FN})/(\text{TP} + \text{TN} + \text{FP} + \text{FN}). \end{aligned} \quad (10)$$

Therefore, Se, Sp, Ac, and Er are calculated to be 100%, 94.7%, 97.2%, and 2.78%, respectively. In short, the accuracy of the proposed snoring recognition method is very high. In fact, the boundary equation can be automatically calibrated periodically, because Q and RR are easy to obtain when awake. There is at least one awake stage during every sleep, so after multiple data acquisitions, the nonsnoring data of awake stages can be applied to adjust the boundary equation automatically, so as to improve the accuracy of snoring recognition.

C. Sleep Stages Classification

Similarly, in order to evaluate the accuracies of sleep stages measured by the sleep monitoring belt, the results measured by PSG are used as the golden standards. There are six stages classified by PSG, namely, awake stage, REM stage, S1 stage, S2 stage, S3 stage, and S4 stage. In general, S1 stage and S2 stage are combined as light sleep stage, while S3 stage and S4 stage are combined as deep sleep stage. Thus, there are four stages in total, namely, awake, REM, light sleep and deep sleep stages. Furthermore, if REM stage, S1 stage, S2 stage, S3 stage, and S4 stage are combined as asleep stage, then there are only two stages in total, namely, awake and asleep stages. Therefore, the two devices are adopted for the sleep tests of the tested person simultaneously, then the performances of 2-stage analysis and 4-stage analysis are evaluated.

The sleep stages predicted by the proposed sleep monitoring belt and detected by PSG within 9 h are illustrated in Fig. 19. The predicted stages and PSG stages are dyed red and blue, respectively. It can be seen that the results of

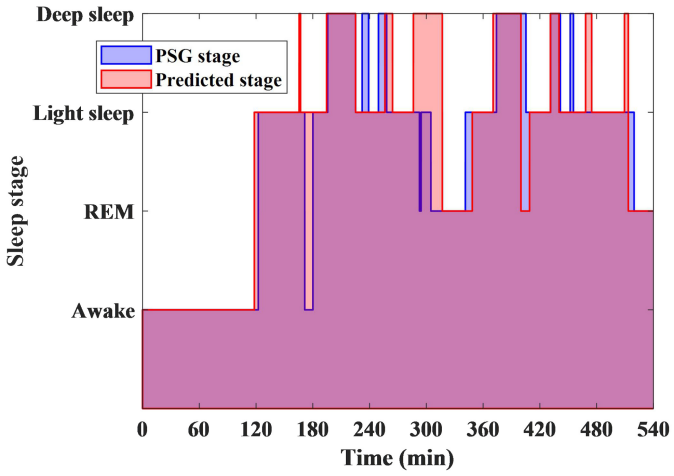

Fig. 19. Analysis results of sleep stages are predicted by the proposed sleep monitoring belt and detected by PSG within 9 h.

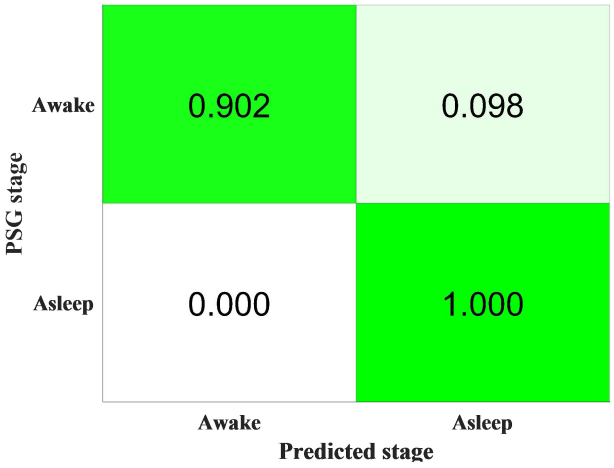

Fig. 20. Performance of the sleep monitoring belt with 2-stage analysis.

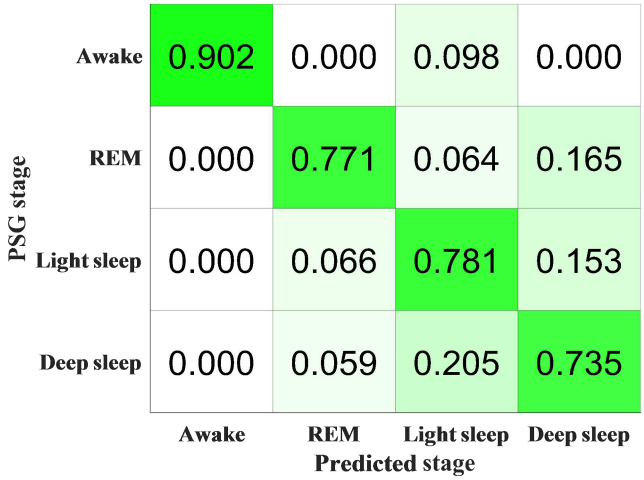

Fig. 21. Performance of the sleep monitoring belt with 4-stage analysis.

TABLE III
PERFORMANCE COMPARISON OF VARIOUS STATE-OF-THE-ART METHODS

Authors	Devices	Accuracy of 4-stage analysis	Accuracy of 2-stage analysis
A. R. Hassan, et al. [46]	EEG	92.89%	98.24%
A. R. Hassan, et al. [47]	EEG	87.49%	95.05%
A. R. Hassan, et al. [48]	EEG	92.14%	99.48%
A. R. Hassan, et al. [49]	EEG	91.48%	98.29%
A. R. Hassan, et al. [50]	EEG	91.2%	97.73%
A. R. Hassan, et al. [51]	EEG	82.83%	91.73%
A. R. Hassan, et al. [52]	EEG	93%	98%
A. R. Hassan, et al. [53]	EEG	92.46%	98.01%
A. R. Hassan, et al. [54]	EEG	92.11%	97.5%
A. R. Hassan, et al. [55]	EEG	94.36%	99.75%
Proposed Method	A flexible belt	79.7%	95.1%

sleep stages analysis obtained by the two sleep monitoring methods are basically the same, and most of the areas are overlapped. Based on Fig. 19 and the similar definition of (10), the performance of the sleep monitoring belt with 2-stage (i.e., awake and asleep stages) analysis is illustrated in Fig. 20. It figures out that the sensitivities of awake and asleep stages are 90.2% and 100%, respectively. Thus, the corresponding accuracy of sleep stages prediction with 2-stage analysis can be calculated, which is as high as 95.1%.

In addition, the performance of the sleep monitoring belt with 4-stage (i.e., awake, REM, light sleep, and deep sleep stages) analysis is illustrated in Fig. 21. It indicates that the sensitivities of awake, REM, light sleep, and deep sleep stages are 90.2%, 77.1%, 78.1%, and 73.5%, respectively. Similarly, the corresponding accuracy of sleep stages prediction with 4-stage analysis can be calculated, which decreases to 79.7%. Although this result is still acceptable, it is not high enough. Compared with the performances reported by Hassan *et al.* [46]–[55], as listed in Table III, the accuracies of 2-stage analysis and 4-stage analysis in this article are a little worse. After all, the proposed classification method of sleep stages is based on body movement, heart rate, and respiration rate measured by the belt, instead of the signals of EEG or PSG, so the analysis deviations are inevitable. Certainly, the performances should be improved by optimizing the classification method in the future.

V. CONCLUSION

In this article, a novel smart flexible sleep monitoring belt with MEMS triaxial accelerometer and pressure sensor is developed to detect vital signs, snore events, and sleep stages. Besides, the related algorithms and methods for data preprocessing, heart and respiration rates detection, snoring recognition, and sleep stages classification are proposed detailedly. The experimental results demonstrate that the detection accuracies of heart rate and respiration rate of the belt are about 1.5 and 0.7 bpm, respectively. The accuracy of 97.2% is achieved by the proposed snoring recognition method. In addition, as for 2-stage analysis, the accuracy of sleep stages prediction is as high as 95.1%. However, as for 4-stage analysis, the accuracy of sleep stages prediction decreases to 79.7%. To sum up, the test results indicate that vital signs detection, snoring recognition, and sleep stages classification based on the sleep monitoring belt are feasible and effective.

Owing to the merits of high performance, low cost, and unobtrusiveness, this smart flexible belt can be widely used for

sleep monitoring at home, and it is very useful for the insomniacs and somebody with OSA. Besides, it can be applied to measure the vital signs of the elderly, and judge whether they are healthy and alive. However, it should be noted that the sleep detection results of the flexible belt can be only used for auxiliary diagnosis, rather than direct medical diagnosis, since it is not a medical device now. Given that the snoring severity and sleep quality vary from person to person, the proposed methods for snoring recognition and sleep stages classification need to be verified and improved repeatedly with a variety of cases of different people. Especially, the accuracy of sleep stages prediction with 4-stage analysis should be further improved by optimizing the classification method based on more parameters. These will be our future work.

REFERENCES

[1] D. C. Yacchirema, D. Sarabia-JáCome, C. E. Palau, and M. Esteve, "A smart system for sleep monitoring by integrating IoT with big data analytics," *IEEE Access*, vol. 6, pp. 35988–36001, 2018.

[2] H. Singh, R. K. Tripathy, and R. B. Pachori, "Detection of sleep apnea from heart beat interval and ECG derived respiration signals using sliding mode singular spectrum analysis," *Digit. Signal Process.*, vol. 104, Sep. 2020, Art. no. 102796.

[3] W. Kalintha, T. Kato, and K. Fukui, "SleepAge: Sleep quality assessment from nocturnal sounds in home environment," *Procedia Comput. Sci.*, vol. 176, pp. 898–907, 2020.

[4] I. Perez-Pozuelo *et al.*, "The future of sleep health: A data-driven revolution in sleep science and medicine," *npj Digit. Med.*, vol. 3, no. 1, p. 42, 2020.

[5] S. Fallmann and L. Chen, "Computational sleep behavior analysis: A survey," *IEEE Access*, vol. 7, pp. 142421–142440, 2019.

[6] S. Roomkham, D. Lovell, J. Cheung, and D. Perrin, "Promises and challenges in the use of consumer-grade devices for sleep monitoring," *IEEE Rev. Biomed. Eng.*, vol. 11, pp. 53–67, Mar. 2018.

[7] C.-T. Lin *et al.*, "IoT-based wireless polysomnography intelligent system for sleep monitoring," *IEEE Access*, vol. 6, pp. 405–414, 2018.

[8] T. Nakamura, V. Goverdovsky, M. J. Morrell, and D. P. Mandic, "Automatic sleep monitoring using ear-EEG," *IEEE J. Transl. Eng. Health Med.*, vol. 5, Jun. 2017, Art. no. 2800108.

[9] T. Nakamura, Y. D. Alqurashi, M. J. Morrell, and D. P. Mandic, "Hearables: Automatic overnight sleep monitoring with standardized in-ear EEG sensor," *IEEE Trans. Biomed. Eng.*, vol. 67, no. 1, pp. 203–212, Jan. 2020.

[10] Y. Bao and S. Yang, "A smartphone-based sleep monitoring model," in *Proc. IPEC*, Dalian, China, 2020, pp. 449–454.

[11] X. M. Chang, C. Peng, G. L. Xing, T. Hao, and G. Zhou, "iSleep: A smartphone system for unobtrusive sleep quality monitoring," *ACM Trans. Sensor Netw.*, vol. 16, no. 3, pp. 1–32, Jul. 2020.

[12] A. Zaffaroni *et al.*, "Sleep staging monitoring based on sonar smartphone technology," in *Proc. EMBC*, Berlin, Germany, 2019, pp. 2230–2233.

[13] C.-K. Weng, J.-W. Chen, P.-Y. Lee, and C.-C. Huang, "Implementation of a wearable ultrasound device for the overnight monitoring of tongue base deformation during obstructive sleep apnea events," *Ultrasound Med. Biol.*, vol. 43, no. 8, pp. 1639–1650, 2017.

[14] S. Jeon, T. Park, A. Paul, Y.-S. Lee, and S. H. Son, "A wearable sleep position tracking system based on dynamic state transition framework," *IEEE Access*, vol. 7, pp. 135742–135756, 2019.

[15] I. Ferrer-Lluis, Y. Castillo-Escario, J. M. Montserrat and R. Jané, "Analysis of smartphone triaxial accelerometry for monitoring sleep-disordered breathing and sleep position at home," *IEEE Access*, vol. 8, pp. 71231–71244, 2020.

[16] C.-E. Kuo, Y.-C. Liu, D.-W. Chang, C.-P. Young, F.-Z. Shaw, and S.-F. Liang, "Development and evaluation of a wearable device for sleep quality assessment," *IEEE Trans. Biomed. Eng.*, vol. 64, no. 7, pp. 1547–1557, Jul. 2017.

[17] J.-Y. Kim, C.-H. Chu, and M.-S. Kang, "IoT-based unobtrusive sensing for sleep quality monitoring and assessment," *IEEE Sensors J.*, vol. 21, no. 3, pp. 3799–3809, Feb. 2021.

[18] A. Tal, Z. Shinar, D. Shaki, S. Codish, and A. Goldbart, "Validation of contact-free sleep monitoring device with comparison to polysomnography," *J. Clin. Sleep Med.*, vol. 13, no. 3, pp. 517–522, 2017.

[19] F. Li, J. Clemente, and W. Song, "Non-intrusive and non-contact sleep monitoring with seismometer," in *Proc. GlobalSIP*, Anaheim, CA, USA, 2018, pp. 449–453.

[20] F. Li, M. Valero, J. Clemente, Z. Tse, and W. Song, "Smart sleep monitoring system via passively sensing human vibration signals," *IEEE Sensors J.*, vol. 21, no. 13, pp. 14466–14473, Jul. 2021.

[21] W. R. Pigeon, M. Taylor, A. Bui, C. Oleynk, P. Walsh, and T. M. Bishop, "Validation of the sleep-wake scoring of a new wrist-worn sleep monitoring device," *J. Clin. Sleep Med.*, vol. 14, no. 6, pp. 1057–1062, 2018.

[22] A. J. Boe *et al.*, "Automating sleep stage classification using wireless, wearable sensors," *npj Digit. Med.*, vol. 2, no. 1, p. 131, 2019.

[23] N. Cellini, E. A. McDevitt, S. C. Mednick, and M. P. Buman, "Free-living cross-comparison of two wearable monitors for sleep and physical activity in healthy young adults," *Physiol. Behav.*, vol. 157, pp. 79–86, Apr. 2016.

[24] N. Yunyoung, K. Yeesock, and L. Jinseok, "Sleep monitoring based on a tri-axial accelerometer and a pressure sensor," *Sensors*, vol. 16, no. 5, p. 750, 2016.

[25] S. Rajala and J. Lekkala, "Film-type sensor materials PVDF and EMFi in measurement of cardiorespiratory signals—A review," *IEEE Sensors J.*, vol. 12, no. 3, pp. 439–446, Mar. 2012.

[26] W. Li, C. Sun, C. Chen, and W. Chen, "Unobtrusive monitoring of cardiorespiratory signals during sleep based on PVDF sensor and singular spectrum analysis," in *Proc. I2MTC*, Houston, TX, USA, 2018, pp. 1–6.

[27] S. Rajala, M. Paajanen, and J. Lekkala, "Measurement of sensitivity distribution map of a ferroelectret polymer film," *IEEE Sensors J.*, vol. 16, no. 23, pp. 8517–8522, Dec. 2016.

[28] G. Matar, G. Kaddoum, J. Carrier, and J.-M. Lina, "Kalman filtering for posture-adaptive in-bed breathing rate monitoring using bed-sheet pressure sensors," *IEEE Sensors J.*, vol. 21, no. 13, pp. 14339–14351, Jul. 2021.

[29] L. Peng, A. Yin, W. Song, W. Yao, H. Ren, and L. Yang, "Sleep monitoring with hidden Markov model for physical conditions tracking," *IEEE Sensors J.*, vol. 21, no. 13, pp. 14232–14239, Jul. 2021.

[30] C. Carlson *et al.*, "Bed-based instrumentation for unobtrusive sleep quality assessment in severely disabled autistic children," in *Proc. EMBC*, Orlando, FL, USA, 2016, pp. 4909–4912.

[31] W. Wang, Z. Pang, L. Peng, and F. Hu, "Non-intrusive vital sign monitoring using an intelligent pillow based on a piezoelectric ceramic sensor," *J. Eng. Fibers Fabrics*, vol. 15, pp. 1–11, Dec. 2020.

[32] L. Rachakonda, S. P. Mohanty, E. Kougianos, K. Karunakaran, and M. Ganapathiraju, "Smart-pillow: An IoT based device for stress detection considering sleeping habits," in *Proc. iSES*, Hyderabad, India, 2018, pp. 161–166.

[33] H. Adil, A. A. Koser, and A. Gupta, "Sleep monitoring using laser blood flowmeter," in *Proc. SCEECS*, Bhopal, India, 2020, pp. 1–4.

[34] Y. Li *et al.*, "Smart optic fiber mattress for animal sleep continuous monitoring based multi-modal interferometer," *J. Lightw. Technol.*, vol. 39, no. 12, pp. 4131–4137, Jun. 2021.

[35] C. Yu, W. Xu, N. Zhang, and C. Yu, "Non-invasive smart health monitoring system based on optical fiber interferometers," in *Proc. ICOCN*, Wuzhen, China, 2017, pp. 1–3.

[36] F. Deng *et al.*, "Design and implementation of a noncontact sleep monitoring system using infrared cameras and motion sensor," *IEEE Trans. Instrum. Meas.*, vol. 67, no. 7, pp. 1555–1563, Jul. 2018.

[37] S. M. Mohammadi, M. R. Alnowami, S. Khan, D.-J. Dijk, A. Hilton, and K. Wells, "Sleep posture classification using a convolutional neural network," in *Proc. EMBC*, Honolulu, HI, USA, 2018, pp. 1–4.

[38] F. Lin *et al.*, "SleepSense: A noncontact and cost-effective sleep monitoring system," *IEEE Trans. Biomed. Circuits Syst.*, vol. 11, no. 1, pp. 189–202, Feb. 2017.

[39] S. Im, H. Kim, C. Lee, and H. Oh, "Implement of sleep monitoring system using UWB, PPG," in *Proc. ICTC*, Jeju-do, South Korea, 2019, pp. 1390–1393.

[40] H. Hong *et al.*, "Microwave sensing and sleep: Noncontact sleep-monitoring technology with microwave biomedical radar," *IEEE Microw. Mag.*, vol. 20, no. 8, pp. 18–29, Aug. 2019.

[41] T. Lauteslager, S. Kampakis, A. J. Williams, M. Maslik, and F. Siddiqui, "Performance evaluation of the circadia contactless breathing monitor and sleep analysis algorithm for sleep stage classification," in *Proc. EMBC*, Montreal, QC, Canada, 2020, pp. 5150–5153.

[42] A. Tataraidze, R. Olesyuk, and M. Pikhletsky, "Can we monitor breathing during sleep via Wi-Fi on smartphone?" in *Proc. EMBC*, Berlin, Germany, 2019, pp. 6710–6713.

[43] Y. Gu, J. Zhan, Z. Liu, J. Li, Y. Ji, and X. Wang, "Sleepy: Adaptive sleep monitoring from afar with commodity WiFi infrastructures," in *Proc. WCNC*, Barcelona, Spain, 2018, pp. 1–5.
[44] Y. Gu, Y. Zhang, J. Li, Y. Ji, X. An, and F. Ren, "Sleepy: Wireless channel data driven sleep monitoring via commodity WiFi devices," *IEEE Trans. Big Data*, vol. 6, no. 2, pp. 258–268, Jun. 2020.
[45] B. Yu *et al.*, "WiFi-sleep: Sleep stage monitoring using commodity Wi-Fi devices," *IEEE Internet Things J.*, vol. 8, no. 18, pp. 13900–13913, Sep. 2021.
[46] M. M. Rahman, M. I. H. Bhuiyan, and A. R. Hassan, "Sleep stage classification using single-channel EOG," *Comput. Biol. Med.*, vol. 102, pp. 211–220, Nov. 2018.
[47] A. R. Hassan, S. K. Bashar, and M. I. H. Bhuiyan, "On the classification of sleep states by means of statistical and spectral features from single channel Electroencephalogram," in *Proc. ICACCI*, 2015, pp. 2238–2243.
[48] A. R. Hassan and M. I. H. Bhuiyan, "Computer-aided sleep staging using complete ensemble empirical mode decomposition with adaptive noise and bootstrap aggregating," *Biomed. Signal Process. Control*, vol. 24, pp. 1–10, Sep. 2016.
[49] A. R. Hassan and M. I. H. Bhuiyan, "Automatic sleep stage classification," in *Proc. EICT*, 2015, pp. 211–216.
[50] A. R. Hassan and M. I. H. Bhuiyan, "Automatic sleep scoring using statistical features in the EMD domain and ensemble methods," *Biocybern. Biomed. Eng.*, vol. 36, no. 1, pp. 248–255, 2016.
[51] A. R. Hassan, S. K. Bashar, and M. I. H. Bhuiyan, "Automatic classification of sleep stages from single-channel electroencephalogram," in *Proc. INDICON*, 2015, pp. 1–6.
[52] A. R. Hassan, S. K. Bashar, and M. I. H. Bhuiyan, "Automated identification of sleep states from EEG signals by means of ensemble empirical mode decomposition and random under sampling boosting," *Comput. Methods Programs Biomed.*, vol. 140, pp. 201–210, Mar. 2017.
[53] A. R. Hassan, S. K. Bashar, and M. I. H. Bhuiyan, "An automated method for sleep staging from EEG signals using normal inverse Gaussian parameters and adaptive boosting," *Neurocomputing*, vol. 219, pp. 76–87, Jan. 2017.
[54] A. R. Hassan, S. K. Bashar, and M. I. H. Bhuiyan, "A decision support system for automatic sleep staging from EEG signals using tunable Q-factor wavelet transform and spectral features," *J. Neurosci. Methods*, vol. 271, pp. 107–118, Sep. 2016.
[55] A. R. Hassan and A. Subasi, "A decision support system for automated identification of sleep stages from single-channel EEG signals," *Knowl. Based Syst.*, vol. 128, pp. 115–124, Jul. 2017.

Chunhua He received the B.S. degree in microelectronics from Sun Yat-sen University, Guangzhou, China, in 2010, and the M.S. and Ph.D. degrees in microelectronics from Peking University, Beijing, China, in 2013 and 2018, respectively.

From 2013 to 2017, he was an Engineer with the No. 5 Electronics Research Institute, Ministry of Industry and Information Technology, Guangzhou. From 2017 to 2019, he was an Engineer with Midea Group, Foshan, China. From 2019 to 2021, he was a Senior Engineer with Guangzhou 37 Degree Smart Home Company Ltd., Guangzhou. He joined the School of Computer, Guangdong University of Technology, Guangzhou, in 2021, where he is currently an Associate Professor. His current research interests include the design and application of MEMS sensors and artificial intelligence algorithms for biomedical engineering.

Jiewen Tan received the B.S. degree in mechanical engineering and the M.S. degree in material processing engineering from the Huazhong University of Science and Technology, Wuhan, China, in 2014 and 2016, respectively.

From 2016 to 2019, he was an Engineer with Midea Group, Foshan, China. He joined Guangzhou 37 Degree Smart Home Company Ltd., Guangzhou, China, in 2019, where he is currently an Engineer. His current research interests include intelligent sleep monitoring and biological information processing.

Xuelei Jian received the B.S. degree in mechanical manufacturing and automation from Wuhan Institute of Technology, Wuhan, China, in 2017, and the M.S. degree in mechanical engineering from Shantou University, Shantou, China, in 2020.

He joined Guangzhou 37 Degree Smart Home Company Ltd., Guangzhou, China, in 2020, where he is currently an Engineer. His current research interests include machine structure design and automatic speech recognition, computer vision, and continuous glucose measurement.

Guangxiong Zhong received the B.S. degree in electronic information engineering from Shantou University, Shantou, China, in 2009. He is currently pursuing the M.S. degree in technology economy and management with the South China University of Technology, Guangzhou, China.

From 2009 to 2015, he was an Engineer with Guangzhou Southern Power Group Technology Development Company Ltd., Guangzhou. From 2015 to 2017, he was an Engineer with Guangdong Hengju Medical Technology Company Ltd., Guangzhou. From 2017 to 2019, he was an Engineer with Midea Group, Foshan, China. He joined Guangzhou 37 Degree Smart Home Company Ltd., Guangzhou, in 2019, where he is currently a Senior Engineer. His current research interests include embedded intelligent product design, design and application of multisensor fusion algorithms, and artificial intelligence algorithms in biomedical engineering.

Lianglun Cheng received the B.S. and M.S. degrees in automatic control engineering from the Huazhong University of Science and Technology, Wuhan, China, in 1988 and 1992, respectively, and the Ph.D. degree in automatic control engineering from the Institute of Automation, Chinese Academy of Sciences, Beijing, China, in 1999.

He joined the School of Computer, Guangdong University of Technology, Guangzhou, China, in 1992, where he is currently a Professor and the Dean. His current research interests include Internet of Things and information physical integration system, interconnection and fusion of heterogeneous network, big data of industrial process, and high performance computing.

Prof. Cheng is currently an expert with special subsidy from the government of the State Council, the Director of the national and local joint Engineering Research Center for Integrated Technology of Intelligent Manufacturing Information Physics Fusion System, the Director of the Key Laboratory of Guangdong Information Physics Fusion System, the Deputy Director of Qian Xuesen Innovation Committee of CASS, the Director of China automation society, a member of China Computer Society, the Vice Director of Guangdong automation society, and an Executive Vice President of Guangdong Robotics Society.

Juze Lin received the B.S. degree in health and rehabilitation of traditional Chinese medicine and the M.S. and M.D. degrees in clinical specialty of integrated Chinese and Western medicine from Guangzhou University of Chinese Medicine, Guangzhou, China, in 2003, 2006, and 2018, respectively.

He joined Guangdong Provincial People's Hospital and Guangdong Institute of Gerontology, Guangdong Academy of Medical Sciences, Guangzhou, in 2006, where he is currently the Deputy Chief Physician of Clinical Specialty of Integrated Chinese and Western medicine with the Department of Traditional Chinese Medicine. His current research interests include the integrated Chinese and Western medicine and biomedical engineering.

Dr. Lin is currently an Editorial board Member of *Journal of Chinese Folk Therapy*; a member of the Professional Committee of Cancer Palliative Care Research, World Federation of Chinese Medicine Societies; the Director of Oncology Medical Professional Committee of Chinese Association of Ethnic Medicine; the Vice Secretary General of Geriatrics Committee of Chinese Association of Ethnic Medicine; the Vice Chairman of Geriatric Disease Prevention Committee of Guangdong Traditional Medical Association; and the Vice President of Guangdong Society of Folk Traditional Chinese Medicine.